

GAS DYNAMICS IN THE CENTRAL CAVITY OF THE HYLIFE-II REACTOR†

Xiang M. Chen, Virgil E. Schrock and Per F. Peterson
Department of Nuclear Engineering
University of California at Berkeley
Berkeley, CA 94720
(510)642-0421

Philip Colella
Department of Mechanical Engineering
University of California at Berkeley
Berkeley, CA 94720
(510)642-2652

ABSTRACT

The HYLIFE-II ICF reactor uses molten salt Flibe (Li_2BeF_4) as liquid blanket material. After the micro-explosion of the D-T capsule in the center of the chamber the emitted x rays ablate a thin layer of the liquid and generate a high temperature plasma. This paper uses a second order Godunov numerical method to solve for the gas dynamics of the ablated material in the central cavity. Because the initial ablation has very small characteristic length scale (about 10 microns), a time varying mesh spacing is adapted. The equation of state for Flibe vapor is used in the calculation along with the parameters for the HYLIFE-II design. The results reveal that the gas dynamic response is sensitive to the initial energy deposition in the liquid and that the two-dimensional shock effects are very important in determining the pressure and density field in the central cavity. By neglecting radiation heat transfer, the current calculation results give a conservative estimation of the shock strength.

INTRODUCTION

In a HYLIFE-II ICF reactor, microexplosion occurs in the center of the central cavity of the reactor chamber about 8 times per second¹. The high energy x rays, debris and neutrons emitted from fusion cause intensive heating of the surrounding liquid Flibe blanket material. The neutrons penetrate deeply into the liquid and induce a fairly uniform volumetric heating throughout the liquid blanket². The x rays are absorbed within a depth of about 10 microns in the liquid. The severe surface heating ablates this layer, which then implodes toward the center cavity. The imploding vapor forms a compressed mass near the centerline of the chamber and converts the kinetic energy back to thermal energy. The resulting high temperature plasma then rebounds toward the liquid blanket while radiating and vaporizing more material off the blanket. This vapor then interacts with the liquid blanket, vents through it and

† Work performed under the auspices of U.S. Department of Energy by the Lawrence Livermore National Laboratory under Contract W-7405-Eng-48

A.1.23

Log. No. E030

The 10th Topic Meeting
of Fusion Technology
Boston, June 7-11, 1988

To be published in
Fusion Technology

finally impacts the structural chamber wall. The magnitude of the vapor impulse imparted to the liquid blanket and impulse onto the chamber wall are key factors in the HYLIFE-II. These factors depend on the gas dynamics in the central cavity and the gas interaction with the liquid blanket geometry^{3,4}. The initial ablation process is challenging in terms of the energy density and the short characteristic time and length scales of the problem. Some previous numerical models^{3,5} for calculating the initial vaporization with a one-dimensional (1-D) Lagrangian method suffer from the lack of accurate treatment of shock phenomena. Numerical diffusion can be observed in the results. Our current effort implements a second order Godunov method into 1-D and 2-D gas dynamics calculations for the HYLIFE-II central cavity. This numerical method is designed for computing shock wave problems. Radiation transport as modeled in ref. 5 is not yet included in the current results, but it will be incorporated in future work.

THE ENERGY DEPOSITION IN THE LIQUID

Of the total yield of the fusion capsule, about one third goes to x rays and debris and two thirds to neutrons⁶. The deposition of neutron energy at the liquid surface is negligible relative to the strong x-ray heating. The intensity of the x rays decreases approximately exponentially into the liquid. The attenuation coefficients depend on the energy level and are different for x rays and debris. After being excited the stopping power of a material decreases. Therefore the attenuation coefficient is a function of both time and position during the deposition. To simplify the problem we assume that the averaged attenuation coefficient is half the attenuation coefficient for the typical fusion x rays in Flibe liquid and consider the deposition as instantaneous. Thus, the energy distribution can be expressed as

$$e(x) = \frac{\phi_0}{4\pi r^2} \lambda e^{-\lambda x} \quad (1)$$

where e (J/m^3) is energy density, ϕ_0 (= 112 MJ) total incident energy, λ ($\sim 9.9 \times 10^{-5} m^{-1}$) the attenuation coefficient, x (m) the distance into the liquid and r (m) the distance between the point of interest and the fusion source.

In the HYLIFE-II reactor, the central cavity has approximately cylindrical geometry with 0.5 m radius and 2 m height (Fig. 1), and the target explodes at the center. The energy fluence into the liquid per unit area at the mid-plane is 5 times greater than at the top and bottom edge. The vaporization of the liquid is governed by the induced energy density. In this calculation, we assume a layer is evaporated which possesses energy greater than the cohesive energy (the combination of the liquid sensible heat and the latent heat). The liquid beneath this layer remains in the liquid state. The thickness of the vaporized layer can then be calculated as

$$\delta = \frac{1}{\lambda} \ln\left(\frac{\lambda \phi_0}{4\pi r^2 \rho e_c}\right) \cos\theta \quad (2)$$

where ρ is the liquid density, θ the x-ray incident angle, $e_c = (T_{\text{sat}} - T_0)C_p + h_{fg}$ the cohesive energy density, T_{sat} and T_0 the saturation and initial temperatures, C_p the liquid specific heat, and h_{fg} the latent heat. It is interesting to mention that

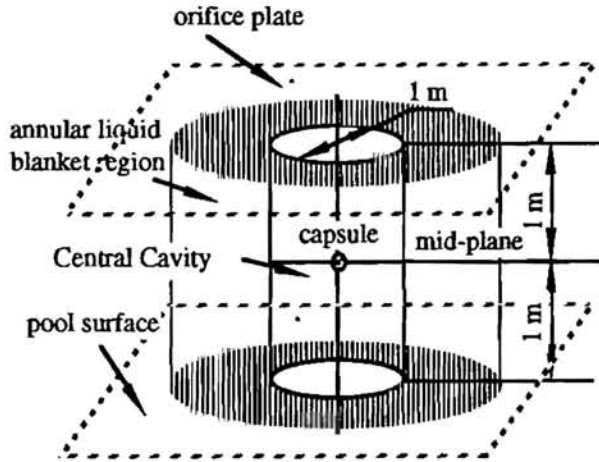


Fig. 1 The central cavity geometry

even though the energy fluence varies by 5 times from mid-plane to the edges along the height of the cylinder, the vaporization thickness is only different by about $\sqrt{5}$. This is because of the change of the incident angle ($\cos\theta$). The distance to the source has very little effect.

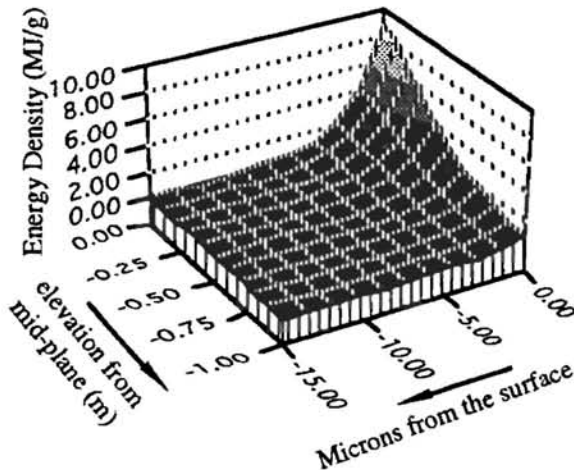


Fig. 2 The energy deposition density inside the liquid

The initial energy density distribution (Fig. 2) in the liquid provides the driving force for the central cavity gas dynamics.

GAS DYNAMICS AND THE SECOND ORDER GODUNOV METHOD

For the compressible flow problem in the central cavity of HYLIFE-II, shock propagation phenomena dominate. The diffusive processes such as heat conduction and viscous effects are negligible over all but the smallest length scales of interest in the reactor. The gas flow is considered isentropic except across a shock front where it obeys the Rankine-Hugoniot relationship⁷.

The 1-D Euler equations for the compressible flow can be expressed as

$$\frac{\partial U}{\partial t} + \frac{\partial F}{\partial x} = 0 \quad (3)$$

where $U = (\rho, \rho u, \rho E)^T$ represents a vector of conserved quantities, i.e., mass, momentum and total energy

$F = (\rho u, \rho u^2 + p, \rho u E + up)^T$ the corresponding fluxes

$E = e + \frac{1}{2}\rho u^2$ the total energy.

Superscript T denotes the transpose of the matrix. With an equation of state which relates the pressure with internal energy and density

$$p = p(\rho, e), \quad (4)$$

this becomes a closed system of equations. For HYLIFE-II, we use an equation of state for Flibe gas⁸ which accounts for chemical dissociation and ionization.

This hyperbolic partial differential equation system can be solved by an explicit numerical method. For this study, we have chosen the second order Godunov¹² Eulerian method as improved by Colella and Glaz⁹. The method can handle shock phenomena readily with excellent numerical diffusion control. Since this second order Godunov method provides the core of our calculation, we describe the method briefly below.

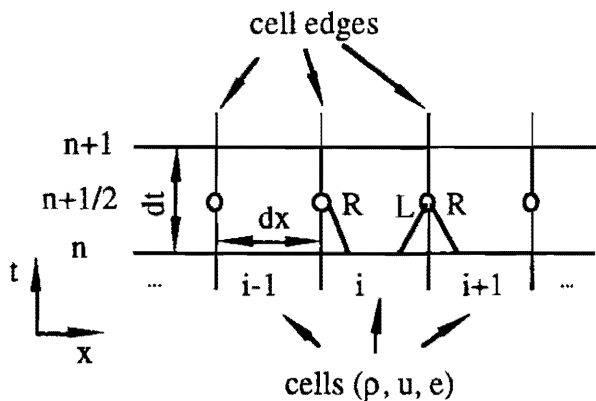


Fig. 3 The cells of the numerical computation

The second order Godunov method is comprised of four steps. In this method, all the quantities such as ρ , u and e are stored as the average in a cell (Fig. 3). As a first step, we interpolate between cells to determine the states of the above quantities at the cell edges at the half time step, i.e.

$$\begin{aligned} q_{i+1/2,L}^{n+1/2} &= q_i^n + \frac{1}{2}(1 - a \frac{dt}{dx}) \Delta q_i \\ q_{i+1/2,R}^{n+1/2} &= q_{i-1}^n - \frac{1}{2}(1 + a \frac{dt}{dx}) \Delta q_{i-1} \end{aligned} \quad (5)$$

where dt is the time step, dx the cell size and a the sound speed. The Δq_i is determined using a van Leer limiter¹⁰. Subscripts L and R stand for the left and right side of a cell edge. For geometries with varying cross sections, such as cylinders and spheres, there is an extra "source" term to be included in the right hand side of the predicted cell edge quantities. It is related with the rate of change of cross sectional area (A) in the flow direction. The source magnitudes are different for ρ , p and e and are listed below:

$$p_{source,i} = - \rho_i \frac{d(\log A)}{dr} u \, dt/2 \quad (6)$$

$$p_{source,i} = \rho_{source,i} a_i^2 \quad (7)$$

$$e_{source,i} = \rho_{source,i} (e_i + p_i/\rho_i)/\rho_i \quad (8)$$

The second step uses a Riemann problem solver. It solves the wave system with discontinuous initial condition q_L and q_R . For gas dynamics, this is a non-linear problem and iteration is generally needed to obtain accurate solutions. It is worth mentioning that even in the rarefaction fan the Riemann solver treats the problem as a discontinuity. Because the Rankine-Hugoniot curve has the same derivatives up to the third order as the isentropic curve⁷, this will not affect the second order accuracy. For details of this gas dynamics Riemann solver refer to Colella⁹ and van Leer¹⁰.

The Riemann solver provides information at the cell edges with which one can easily calculate the fluxes crossing the cell edge in the time step, i.e.

$$F_{i+1/2}^n = F(\rho_{i+1/2} u_{i+1/2}, \rho_{i+1/2} u_{i+1/2}^2 + p_{i+1/2}, \rho_{i+1/2} u_{i+1/2} E + u_{i+1/2} p_{i+1/2})^T \quad (9)$$

Finally, with these fluxes the conserved quantities in every cell can be updated for the new time step according to the weak solution:

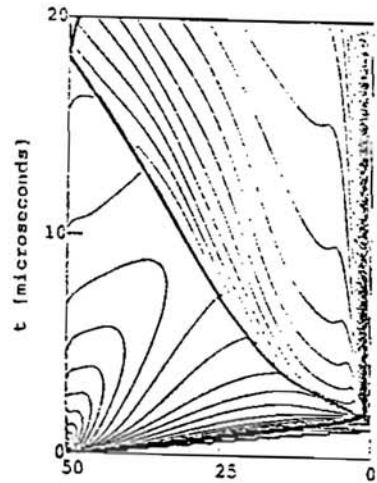
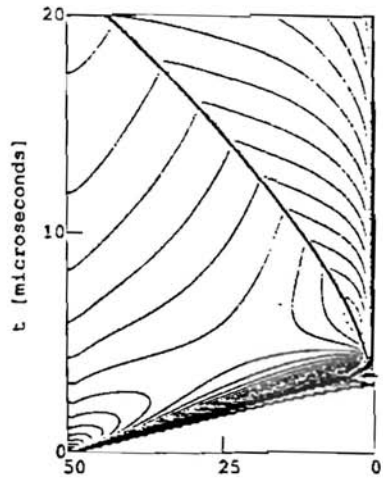
$$U_i^{n+1} = U_i^n + \frac{dt}{dx} (F_{i-1/2}^n - F_{i+1/2}^n) \quad (10)$$

The stability condition of the explicit method requires that the Courant number (adt/dx ; note: dt , dx are time step and grid size here) be less than unity. The boundary for this

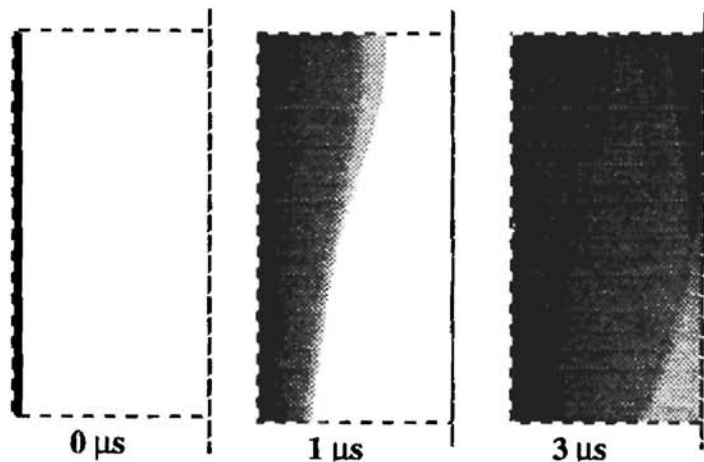
method can be a reflecting wall (possibly oblique to the calculating direction), an open side or a flux control boundary. In the HYLIFE-II cavity problem all boundaries (including planes/line of symmetry) are insulated impermeable walls.

TREATMENT OF VARIABLE MESH SPACING AND THE COMPUTATIONAL DOMAIN

The above formulation and procedures were written out for a 1-D geometry. For 2-D calculations, an operator splitting method¹¹ was applied. The method separates the computation into two sweeps, one in each direction. Each sweep computes one-dimensional shock interactions and



the initial pressure distribution in the ablated material corresponding to the energy distribution. For the exponential distribution case, the particles at the surface possess the highest energy and therefore highest pressure. This gives the shock front a higher speed than the case with uniform energy deposition. Close to the bottom of the ablated layer, the vapor possesses very little excess energy. The bottom particles come off the liquid with very small velocity; they can not catch up with the initial shock but run into the reflected shock at a place close to the liquid surface. However, if the initial energy distribution is uniform inside the ablated layer, the particles in this layer will come off with the same driving pressure, the whole ablated mass follows the shock front fairly closely and very little material remains close to the liquid surface.



shows that the reflected shock takes longer to reach the cavity edge (liquid surface) than in the 1-D calculation. Clearly the pressure relaxation in the axial direction contributes to this. The gas density, velocity, pressure and temperature distribution at the instant of impact against the jets is of particular interest for subsequent calculations of venting and condensation. Figures 6 through 9 plot the quantities at the instant just before the shock impact. From the profiles at three different elevations, one can see that the pressure and density at the top and bottom planes are actually higher than those at the mid-plane. This surprising result occurs due to wave propagation and reflection in the axial direction. These 2-D effects are very strong in this central cavity problem.

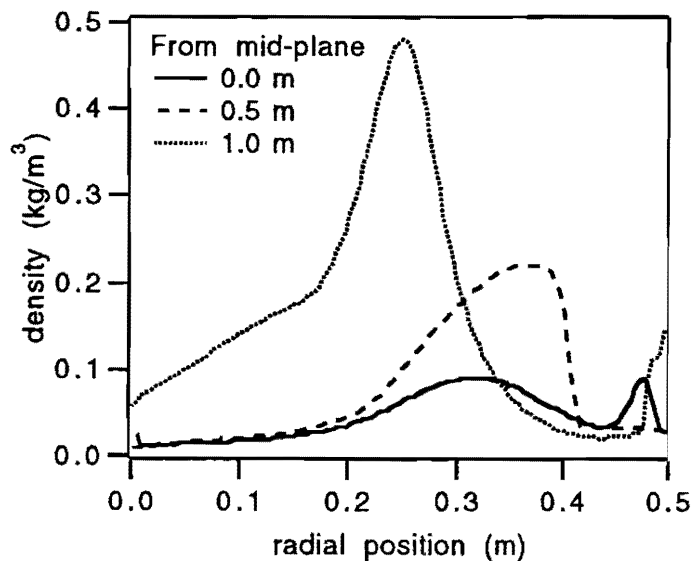


Fig. 6 The density profiles at 23.5 μ s at different elevations

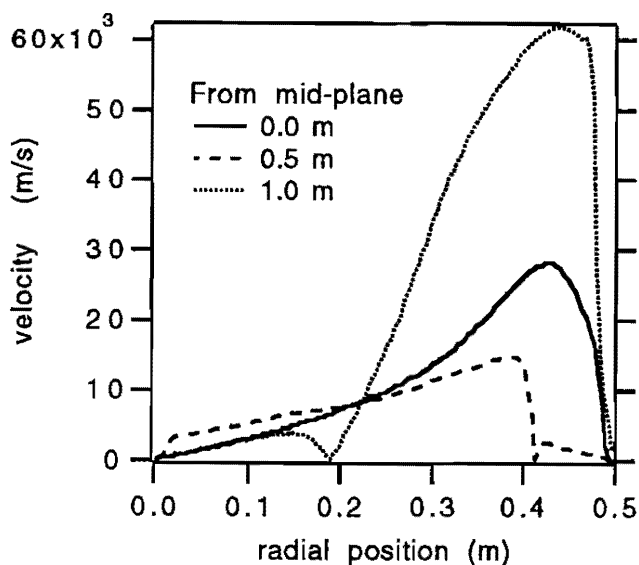


Fig. 7 The velocity profiles at 23.5 μ s at different elevations

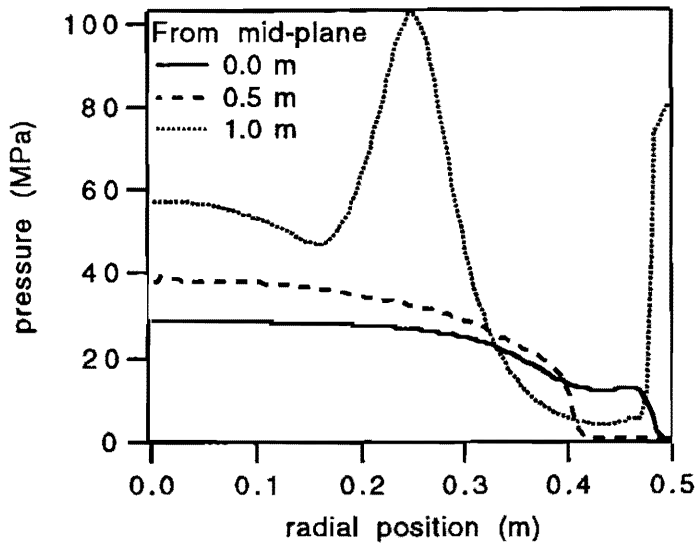


Fig. 8 The pressure profiles at 23.5 μ s at different elevations

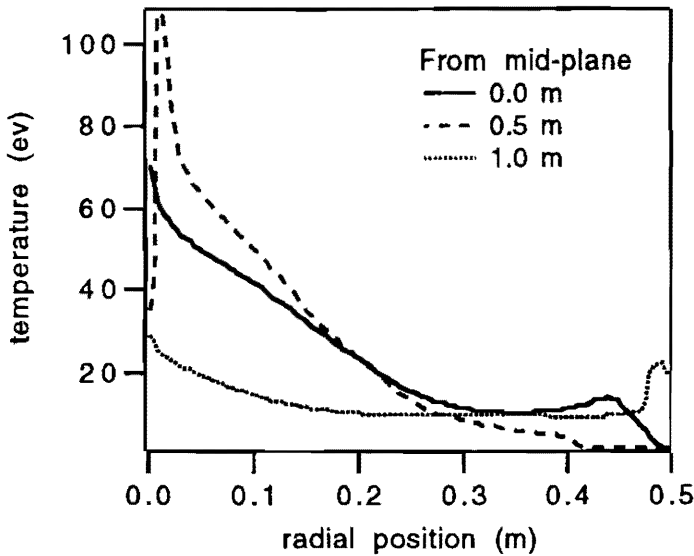


Fig. 9 The temperature profiles at 23.5 for different elevations

DISCUSSION AND CONCLUSIONS

Our results show that the time lapse for the shock front rebounding back to the liquid surface is about 17 μ s for the 1-D exponential initial energy deposition case, 22 μ s if energy deposition is assumed uniform in the vaporized layer and, for the 2-D case, 23.5 μ s due to the relaxation in the axial direction. The strong 2-D shock reflection on the top plane suggests that a careful design is required for the orifice plate.

The gas dynamics is highly sensitive to the initial energy distribution inside the liquid, although the layer ablated initially is extremely thin relative to the total cavity radius. This tells us that the assumption of a uniform initial

energy distribution could result in significant of error. A more accurate detailed model of the initial x ray energy deposition and debris energy absorption by the vapor and liquid therefore deserves careful pursuit.

During the course of wave propagation in the central cavity, the temperature of the vapor is very high. Therefore radiation is certainly important. The current results, we think, should reveal the shock interaction and wave propagation time scale phenomena fairly well, but underestimate the total mass evaporated and consequently predict higher temperatures in general than with radiation transport included.

Comparing with the previous results³ for the HYLIFE-I reactor made with a Lagrangian numerical method, our results have similar pressure and temperature profiles qualitatively, but our density profile does not have a high density annulus close to the liquid surface. That, we think, is partially due to neglecting radiation.

From the results we can see that the current numerical code can preserve the shock front very well and it is also capable of dealing with complex reflecting boundary conditions and the real gas equation of state in the Riemann solver. With the inclusion of the radiation calculation, this code should be able to compute the gas dynamics process in complicated geometries and, of course, in the HYLIFE-II central cavity.

REFERENCES

1. R.W. Moir, "HYLIFE-II Inertial Fusion Energy Power Plant Design," Accepted to the 10th Topic Meeting on the Technology of Fusion Energy, Boston, June 7-11 and to be published in *Fusion Technology* (1992).
2. X. M. Chen and V. E. Schrock, "The Pressure Relaxation of Liquid Jets after Isochoric Heating," *Fusion Technology*, **19**, 721 (1991).
3. L. A. Glenn, "Divergent Impulsive Crossflow Over Packed Columnar Array," *Nucl. Eng. Design*, **56**, 429 (1980).
4. J.C. Liu, P.F. Peterson and V. E. Schrock "Blast Venting through Blanket Material in the HYLIFE ICF reactor," 10th Topic Meeting on the Technology of Fusion Energy, Boston, June 7-11 and to be published in *Fusion Technology* (1992).
5. R. R. Peterson, Joseph J. MacFarlane and Gregory A. Moses, "CONRAD - A Combined Hydrodynamics-Condensation/Vaporization Computer Code", UWFDM-670, Fusion Technology Institute, University of Wisconsin (1988).
6. R.W. Moir, et. al., "HYLIFE-II Progress Report," Lawrence Livermore National Laboratory, University of California, UCID-21816 (1991).
7. Ya. B. Zel'dovich and Yu. P. Raizer, *Physics of Shock Waves and High-Temperature Hydrodynamic Phenomena*, Volume I, pp.63, Academic Press, Inc (1966).
8. X. M. Chen, P.F. Peterson and V. E. Schrock, "Fitted Equation of State for Flibe Gas," UCB-NE- 4190,

Department of Nuclear Engineering, University of California (1992).

9. P. Colella and H. M. Glaz, "Efficient Solution Algorithms for the Riemann Problem for Real Gases," *J. of Comp. Phys.* **59**, 264 (1985).
10. B. van Leer, "Towards the Ultimate Conservative Difference Scheme. V. A Second-Order Sequel to Godunov's Method," *J. of Comp. Phys.* **32**, 101 (1979).
11. G. Strang, "On the Construction and Comparison of Difference Schemes," *SIAM J. Numer. Anal.* **5**, 506 (1968).
12. R.J. LeVeque, *Numerical Methods for Conservation Laws*, Birkhauser Verlag, Basel·Boston·Berlin, pp.138 (1990).

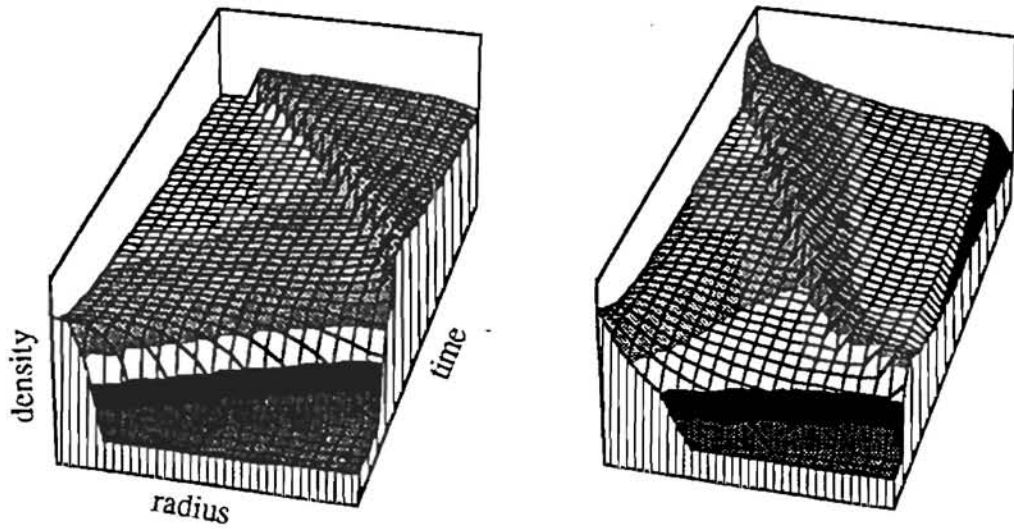
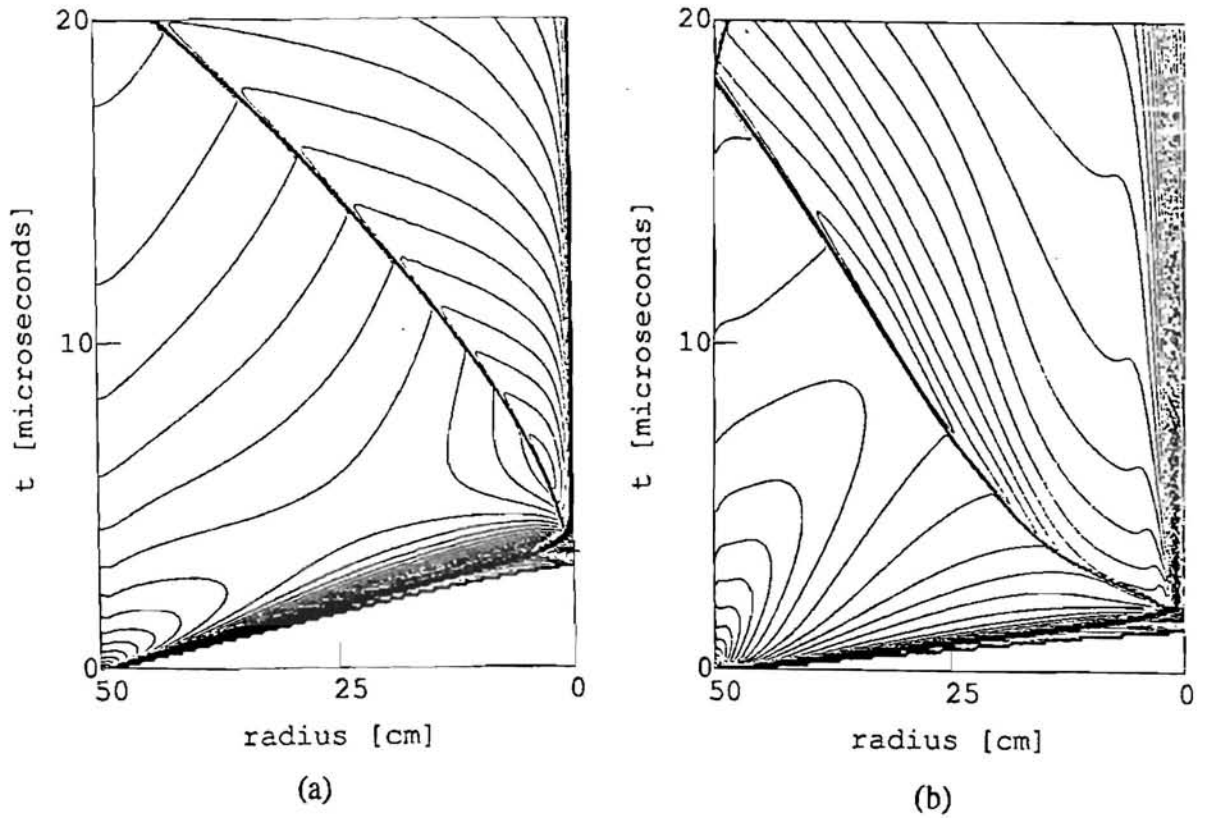


Fig. 4 The contours and profiles of vapor density and the 3-D graphs corresponding to the contour plots. Densities are shown in logarithmic scale (Yield = 350 MJ, in HYLIFE-II geometry)

(a) The initial energy deposition is assumed to be uniform with the ablated layer.

(b) The energy deposition obeys exponential function